

1 High-throughput functional mapping of variants in an arrhythmia gene, *KCNE1*, reveals novel 2 biology

4 **Authors:** Ayesha Muhammad,^{1,2} Maria E. Calandranis,³ Bian Li,³ Tao Yang,³ Daniel J. Blackwell,³
5 M. Lorena Harvey,³ Jeremy E. Smith,³ Ashli E. Chew,³ John A. Capra,⁴ Kenneth A. Matreyek,⁵
6 Douglas M. Fowler,⁶ Dan M. Roden,^{*,1,3,7,8} and Andrew M. Glazer.^{*,1,3}

8 Affiliations:

22 8. Department of Pharmacology, Vanderbilt University Medical Center, Nashville, TN
23 37232, USA.

24

25 * These authors contributed equally.

26 Correspondence: Andrew M. Glazer andrew.m.glazer@vumc.org.

27 Word count:

28 Abstract: 204/250 words

29 Manuscript: 6,738 words (excluding abstract, figure legends and references)

30

31 Keywords: Multiplexed assay of variant effect, long QT syndrome, KCNE1, ion channel,
32 arrhythmia

33 **Abstract**

34 **Background:**

35 *KCNE1* encodes a 129-residue cardiac potassium channel (I_{Ks}) subunit. *KCNE1* variants are
36 associated with long QT syndrome and atrial fibrillation. However, most variants have
37 insufficient evidence of clinical consequences and thus limited clinical utility.

38

39 **Results:**

40 Here, we demonstrate the power of variant effect mapping, which couples saturation
41 mutagenesis with high-throughput sequencing, to ascertain the function of thousands of
42 protein coding *KCNE1* variants. We comprehensively assayed *KCNE1* variant cell surface
43 expression (2,554/2,709 possible single amino acid variants) and function (2,539 variants). We
44 identified 470 loss-of-surface expression and 588 loss-of-function variants. Out of the 588 loss-
45 of-function variants, only 155 had low cell surface expression. The latter half of the protein is
46 dispensable for protein trafficking but essential for channel function. 22 of the 30 *KCNE1*
47 residues (73%) highly intolerant of variation were in predicted close contact with binding
48 partners KCNQ1 or calmodulin. Our data were highly concordant with gold standard
49 electrophysiological data ($\rho = -0.65$), population and patient cohorts (32/38 concordant
50 variants), and computational metrics ($\rho = -0.55$). Our data provide moderate-strength evidence
51 for the ACMG/AMP functional criteria for benign and pathogenic variants.

52

53 **Conclusions:**

54 Comprehensive variant effect maps of *KCNE1* can both provide insight into I_{K_s} channel biology
55 and help reclassify variants of uncertain significance.

56

57 Keywords:

58 *KCNE1*, saturation mutagenesis, multiplexed assay of variant effect, long QT syndrome, variant
59 classification

60

61

62 **Background**

63 Loss-of-function variants in *KCNE1* can cause type 5 long QT syndrome (LQT5; MIM
64 613695), a cardiac arrhythmia disorder characterized by QT prolongation on the
65 electrocardiogram and an increased risk of sudden cardiac death.¹ Heterozygous LQT5 variants
66 can cause isolated QT prolongation (also known as Romano-Ward Syndrome),² and
67 homozygous and compound heterozygous variants can cause both QT prolongation and
68 deafness (Jervell and Lange-Nielsen Syndrome; MIM 612347).³ Almost 50 unique *KCNE1*
69 variants have been observed in patients with LQT5.^{1,4–6} In addition, two gain-of-function
70 variants have been associated with atrial fibrillation in isolated families.⁷ *KCNE1* encodes a
71 single-spanning transmembrane protein that acts as a modulatory subunit to the pore-
72 conducting KCNQ1 to form the I_{Ks} channel critical for cardiac repolarization (Figure 1A). The I_{Ks}
73 complex is conventionally thought of as comprising *KCNE1* and KCNQ1. However, additional
74 proteins, including calmodulin, interact with the complex to modulate channel
75 electrophysiology.⁸ *KCNE1* variants can disrupt channel function in two major ways: by reducing
76 cell surface expression or by altering gating to reduce potassium flux.⁹

77 The American College of Medical Genetics and Genomics/Association of Molecular
78 Pathology (ACMG/AMP) criteria are used to classify variants as pathogenic, likely pathogenic,
79 likely benign, or benign.¹⁰ Variants with inconclusive evidence for clinical classification are
80 designated as variants of uncertain significance (VUS). For many Mendelian disease genes,
81 including *KCNE1*, most discovered variants are VUS and thus have limited impact on clinical
82 decision-making,¹⁰ presenting a major challenge to genomic medicine.^{11,12} In the ClinVar
83 database of variant classifications,¹³ 77.4% of *KCNE1* variants are either VUS or have conflicting

84 interpretations (Figure 1B). These variants, together with those reported by gnomAD or clinical
85 case studies, represent a small subset of all possible missense variants (Figure 1C). It has been
86 proposed that all missense variants compatible with life likely already exist in ~50 individuals on
87 the planet.¹⁴ In the ACMG/AMP scheme, well-validated *in vitro* functional studies can provide
88 up to strong-level evidence for the PS3 (damaging effect on protein) and BS3 (no damaging
89 effect) criteria.^{15,16} However, functional assessment lags behind the rate of VUS discovery due
90 to the rapid increase of genetic testing in research and clinical domains.¹² One way to address
91 this VUS problem is to leverage multiplexed assays for variant effects (MAVEs) to test
92 thousands of variants in a single, highly-multiplexed experiment.^{12,17} In a MAVE, a
93 comprehensive variant library is coupled to a selection assay and high-throughput sequencing
94 to ascertain variant function.

95 In this study, we conducted multiplexed assays of variant cell surface expression and
96 potassium flux on a library of 2,592 single residue KCNE1 variants (95.7% of 2,709 total possible
97 variants, Figure S1). We used an HA epitope in KCNE1 to determine cell surface expression of
98 2,554 individual variants using a “landing pad” cell line,¹⁸ which integrates a single variant per
99 cell. This assay identified 470 missense variants that decrease and 310 that increase cell surface
100 expression. We also used a gain-of-function KCNQ1 variant to design a cell survival assay that
101 selects against cells with functioning channels. We deployed the function assay on 2,539 KCNE1
102 variants and found 588 loss-of-function missense variants, only 155 of which also had low cell
103 surface expression. These datasets correlate well with previously validated *in vitro* studies,
104 computational predictors, population metrics, and clinical phenotypes. Our data provide insight

105 into KCNE1 structure and biology and can be implemented to reclassify variants in the
106 ACMG/AMP scheme.

107

108 **Results**

109

110 ***Validation of an extracellular KCNE1 HA tag to detect cell surface expression***

111 We cloned a 9-residue hemagglutinin (HA) tag into the extracellular domain of *KCNE1*
112 (between residue 33 and 34; Figure 1A). *KCNE1-HA* (33-34) resulted in 3-fold higher cell surface
113 labeling of the I_{Ks} channel complex compared to a previously described HA tag located in a
114 predicted alpha helix (Figure S2A).¹⁹ Neither I_{Ks} peak and tail current densities, nor
115 activation/inactivation properties were significantly different between *KCNE1-WT* and *KCNE1-*
116 *HA* (Figure 1D). Human Embryonic Kidney (HEK) 293T landing pad cells expressing *KCNE1-HA*
117 were labeled with a fluorophore-conjugated anti-HA antibody, visualized by confocal
118 microscopy, and quantified by flow cytometry (Figures 1E and 1F). In cells expressing *KCNE1-HA*
119 only, minimal plasma membrane anti-HA labeling was present, consistent with previous
120 studies.^{9,20} In contrast, cells co-expressing both *KCNE1-HA* and *KCNQ1* demonstrated
121 substantial plasma membrane anti-HA labeling in live cells, and both plasma membrane and
122 intracellular labeling in permeabilized cells (Figure 1E).^{9,21} Quantification of cell surface
123 expression by flow cytometry confirmed these observations (Figure 1F). A minimal but
124 detectable amount of plasma membrane labeling was seen in *KCNE1-HA* only cells but the
125 addition of *KCNQ1* caused a 6.1-fold increase in cell surface expression (Figures 1F and S2B). As
126 expected, a known loss-of-trafficking variant (L51H) had minimal cell surface expression and a

127 known gating variant (D76N) had near-WT cell surface expression when co-expressed with
128 *KCNQ1* (Figures 1F and S2B).²²

129

130 ***A comprehensive library of KCNE1 mutations***

131 We generated a comprehensive variant library of the 129-residue KCNE1 protein
132 associated with random 18-mer barcodes using inverse PCR mutagenesis with degenerate
133 primers (See *Methods*, Figure S3A).²³ We linked 80,282 barcodes to 2,368 missense, 100
134 synonymous, and 124 nonsense KCNE1 variants (95.7% of the total possible variants; Figure
135 S3B). Each variant was represented by a mean of 31 barcodes (Figure S3C).

136

137 ***Multiplexed assay of KCNE1 cell surface expression***

138 We coupled antibody labeling of the extracellular HA tag to deep sequencing of the
139 library barcodes to perform a multiplexed assay of KCNE1 cell surface expression in cells
140 engineered to constitutively express *KCNQ1* (Figure 2A). After quality control (see *Methods*;
141 Figure S4A), we obtained cell surface trafficking scores for 98 synonymous, 117 nonsense, and
142 2,339 missense variants (94.2% of all possible variants; Figure 2B). Scores calculated from three
143 individual replicates were highly concordant (Spearman's $\rho = 0.81\text{-}0.87$, $p < 0.001$; Figure S4B).
144 Cell surface trafficking scores for synonymous variants were normally distributed (0.988-1.024,
145 95% CI, Figures 2B-C). Nonsense variant scores were bimodally distributed (mode 1 = 0.01,
146 mode 2 = 0.74). Nonsense variants from residue 1 to 55 were all trafficking-deficient, whereas
147 nonsense variants at or after residue 56 had near-WT or higher than WT cell surface expression
148 ($p = 2.5 \times 10^{-20}$, Wilcoxon test; Figures 2B-C). We therefore classified nonsense variants as early

149 nonsense (residue 1-55) and late nonsense (56-129) in all subsequent trafficking analyses. All
150 variants at residue 1 were trafficking-null as expected.

151 Missense variants with score estimates (95% confidence interval) lower than 2.5th
152 percentile or higher than 97.5th percentile of the synonymous variant distribution were
153 assigned as loss- or gain-of-trafficking respectively. Using these cutoffs, we identified 470 loss-
154 of-trafficking variants and 311 gain-of-trafficking variants. We also compared trafficking scores
155 to the few literature reports of cell surface trafficking measurements, typically reported as
156 “normal” or “loss-of-trafficking.” 7/9 variants were concordant: 6 variants with normal or near-
157 normal trafficking (T6F, S74L D76A, D76N, Y81C, and W87R) and 1 loss-of-trafficking variant
158 (L51H; Figure S4C).^{22,24-26} Two discordant variants, R98W and G52R, were previously reported
159 to have normal trafficking but were loss-of-trafficking in our assay.⁹

160 Several interesting and previously unreported findings emerged from the cell surface
161 trafficking scores (Figure 2F). As mentioned above, nonsense variants after residue 55 were still
162 able to traffic to the cell surface. In the extracellular N-terminus, almost all cysteine variants
163 from residue 2 to 33 had increased cell surface expression. Residues 46-59 in the
164 transmembrane helix, likely juxtaposed to the hydrophobic core of the lipid bilayer, were highly
165 resistant to polar or charged variation. Variants in residues 61-70, interacting with the
166 intracellular hydrophilic edge of the cell membrane, increased cell surface expression. Predicted
167 alpha helices in the intracellular C-terminus (residues 79-114) had multiple residues resistant to
168 aromatic or larger aliphatic variation.

169 As HEK293T cells only expressing KCNE1 exhibited detectable levels of anti-HA staining,
170 we conducted a second MAVE of KCNE1 cell surface expression in the absence of co-expressed

171 KCNQ1 ("KCNQ1-"; Figure S5) to explore their intermolecular interaction. Trafficking scores for
172 missense variants in the presence and absence of *KCNQ1* were highly correlated (Figure 2D,
173 Spearman's $\rho = 0.88$, $p < 2 \times 10^{-6}$), except for variants in the N-glycosylation sequons (NXS/NXT
174 motifs) at positions 5-7 and 26-28 in the extracellular N-terminus of KCNE1.^{26,27} Most variants
175 disrupting N-glycosylation especially at residues 26 and 28 reduced cell surface expression in
176 the absence of KCNQ1 (Figure 2D). Thus, loss of N-terminal glycosylation is more advantageous
177 to cell surface expression in the presence of KCNQ1. Cell surface expression of cysteine super-
178 trafficking variants (including at the 5-7 and 26-28 glycosylation sequons) was not affected by
179 KCNQ1. As discussed below, this result may reflect antagonism between KCNE1 N-glycosylation
180 and KCNE1/KCNQx interaction unique to KCNQ1 and not other binding partners possibly
181 expressed in HEK293T cells.

182

183 ***Development of a cell fitness assay for KCNE1 function***

184 Since I_{Ks} channels are closed at the resting potential of HEK293T cells (approximately -25
185 mV),²⁸ we developed an assay for KCNE1 function by leveraging the electrophysiology of a
186 previously described gain-of-function variant, KCNQ1-S140G.^{29,30} In the presence of KCNE1,
187 KCNQ1-S140G left-shifts the voltage of I_{Ks} channel activation²⁹ and reduces channel
188 deactivation;³¹ in the absence of KCNE1, the channel expresses minimal current (Figure 3A).
189 These electrophysiological shifts result in substantial KCNE1-dependent K⁺ efflux at -25 mV. We
190 hypothesized that long-term expression of I_{Ks} channels formed by KCNQ1-S140G and normally
191 functioning KCNE1 would decrease cell fitness due to continual K⁺ efflux. To test this
192 hypothesis, we integrated a 1:1 mixture of empty vector control and either wild-type KCNE1-HA

193 or previously studied KCNE1 variants into HEK293T landing pad cells stably expressing KCNQ1-
194 S140G (LP-KCNQ1-S140G, Figure 3B). We then quantified KCNE1⁺ and KCNE1⁻ cell proportions
195 over 20 days (Figure 3C and 3D). Compared to cells with empty vector controls, cells with WT
196 KCNE1 depleted over time, whereas cells with loss-of-function KCNE1 variants (L51H or D76N)
197 persistently survived. Two previously described KCNE1 gain-of-function variants (G60D and
198 G25V)⁷ depleted at the same rate as KCNE1-HA-WT (Figure 3D), indicating that this assay does
199 not distinguish gain-of-function variants from WT.

200

201 ***Multiplexed assay of KCNE1 function***

202 We used this KCNQ1-S140G-based cell fitness assay to conduct a multiplexed assay of
203 KCNE1 function. We integrated the KCNE1 library into HEK293T cells stably expressing KCNQ1-
204 S140G and quantified cell survival over 20 days (Figure 4A). After 20 days, cell expressing
205 synonymous variants were depleted and those expressing most nonsense variants persistently
206 survived (Figure S6A). These changes in the cell pool were not seen in the presence of WT-
207 KCNQ1 (Figure S6B). Variant depletion from day 0 to day 20 was used to calculate normalized
208 KCNE1 function scores for 98 synonymous, 121 nonsense, and 2,320 missense variants (93.7%
209 of all variants; Figures 4B and S6C). Function scores across three replicates were highly
210 concordant (Spearman's $p=0.87$; Figure S6D). Synonymous variants followed an asymmetric
211 unimodal distribution (median = 0.99, IQR=0.27, Figure 4B). Nonsense variants were bimodally
212 distributed (mode 1 = 0.02, mode 2 = 0.99); nonsense variants at residues 1-104 were loss-of-
213 function, whereas nonsense variants at residue 105-129 had WT-like function ($p = 2.6 \times 10^{-13}$,
214 Wilcoxon test, Figure 4C). Thus, across the trafficking and function assays, three classes of

215 nonsense variants were present based on residue number: #1-55 caused loss of trafficking and
216 function, #56-104 caused WT-like or elevated trafficking but loss-of-function, and #105-129
217 caused near WT-like trafficking and function (Figure S7A). All variants at residue 1 were loss-of-
218 function as expected. Missense variant function scores were bimodally distributed (mode 1 =
219 0.14, mode 2 = 1.04). The two modes approximately corresponded to the peaks of the
220 synonymous distribution and early nonsense distributions. Upon comparing trafficking and
221 function scores for missense variants, we found 136 trafficking-null and 288 trafficking-normal,
222 functionally deleterious variants (Figure 4D). We refer to the latter as “gating variants.”

223 On the heatmap of KCNE1 function scores, variation-resistant regions were located in
224 the transmembrane helix (residues 61-73) and the transmembrane-proximal cytosolic alpha
225 helix (residues 77-82; Figure 4F). Known trafficking-null variants (L51H) and gating variants
226 (D76N, W87R) had deleterious function scores.²² Common polymorphisms (G38S, D85N) had
227 WT-like trafficking and function scores, consistent with their minimal effects on baseline QT
228 interval. Residue 85 is otherwise resistant to variation and D85N is only one of 2 missense
229 variants at this residue with WT-like score estimates (D85N: 0.79-1.02, and D85E: 0.69-0.98,
230 95% confidence interval). Variants that disrupted glycosylation sequons (residues 5-7 and 26-
231 28) largely did not alter channel function despite their effects on KCNE1 trafficking (Figure S7B),
232 consistent with previous work.^{26,27} Additionally, N-terminal cysteine residues, while gain-of-
233 trafficking, did not drastically affect function. This is expected, as the assay is not well-powered
234 to detect gain-of-function variants. Only one variant (Y107R) met the “gain-of-function” criteria
235 (score estimate > 97.5% percentile of synonymous scores) and was validated by manual patch
236 clamp (Figure S7C).^{26,27}

237

238 ***Structural model of the KCNE1/KCNQ1/calmodulin complex***

239 An experimental structure of the KCNE1/KCNQ1/calmodulin complex has not been
240 determined, so we examined multiple AI-based models (Figure S8). Aligning predicted
241 structures of KCNE1 to a reported cryo-EM structure of the KCNQ1-KCNE3 complex indicated
242 that the conformation obtained from AlphaFold-multimer modeling (See Supplemental
243 Methods) was likely the most biologically meaningful (Figures 1A and 5). We therefore overlaid
244 mean trafficking and functional scores on the AlphaFold-multimer structural model of the
245 KCNE1-KCNQ1-calmodulin complex (Figure 5A-D). As discussed above, the hydrophobic core of
246 the transmembrane helix (residues 44 to 60) did not tolerate polar or charged variation in both
247 trafficking and function maps. Multiple variants in the cytosolic membrane-proximal region of
248 the transmembrane domain (residues 61-70) increased cell surface expression but were
249 functionally intolerant to variation. This region contains contacts with KCNQ1, including KCNE1
250 residues M62, Y65, and S68 (Figure 5F). Thus, variation in this region likely disrupts normal
251 gating properties of the I_{Ks} channel. Polar and charged variation in an additional predicted
252 intracellular helix (residues 85-105 including functionally constrained residues F78, Y81, I82,
253 and W87) preserved cell surface expression. However, the helix was functionally intolerant to
254 variation likely due to observed interaction with calmodulin (Figure 5G) that affects gating
255 properties of the I_{Ks} complex. Overall, of the 30 KCNE1 residues highly intolerant of variation
256 (>70% of missense variants at given residue position are loss-of-function), 22 (73%) were in
257 close contact ($<5\text{\AA}$) with KCNQ1 (14 residues) and/or calmodulin (9 residues; residue 77 was in
258 close contact with both proteins). These variation-resistant residues comprise 40% of 55 KCNE1

259 residues in close contact with KCNQ1 and/or calmodulin. On the other hand, none of the 70
260 residues where >50% of the missense variants had WT-like functional scores were in close
261 contact with either KCNQ1 or calmodulin.

262

263 ***Correlation of MAVE scores with patch clamp and patient data***

264 We curated a list of 149 *KCNE1* variants with previously published patch clamp,
265 trafficking and patient data, (Additional File 1) and conducted additional patch clamp studies of
266 15 variants (Table S1). The MAVE function scores were strongly correlated with measured or
267 reported peak currents ($p = 1.5 \times 10^{-9}$, $p = 0.65$, $n = 71$; Figure 6A). 26/29 variants with $\leq 25\%$ of
268 WT peak current had deleterious function scores. Only 8 of these 26 had deleterious trafficking
269 scores (30.8%; Figure S9A). 21/29 variants with $> 50\%$ WT peak current had WT-like function
270 and trafficking scores. Although function scores correlated best with peak current, *KCNE1*
271 variants with large shifts in the voltage or time kinetics of activation or deactivation were also
272 more likely to have deleterious scores (Figures 6B and S9B). The trafficking scores had weaker
273 correlations with patch clamp parameters (Figures S9C and S9D). Single nucleotide variants
274 (SNVs) achieved by transversion mutations were more likely to be functionally deleterious
275 compared to variants achieved by transition mutations ($p = 2.2 \times 10^{-4}$, Wilcoxon test; Figures S9E
276 and S9F).

277 We examined the distribution of missense variant scores in presumed normal and
278 pathogenic variants, curated from gnomAD, ClinVar and our literature review of LQT5 and JLNS
279 cases. Variants achieved by more than one single SNV or not present in gnomAD tended to have
280 deleterious function scores ($p = 9.3 \times 10^{-6}$, Wilcoxon test in Figure 6B; $p = 4.6 \times 10^{-5}$, Wilcoxon test

281 in Figure 6C; and Figure S10A). Function scores were largely concordant with clinical outcomes:
282 7/7 ClinVar benign/likely benign variants and 16/19 presumed normal variants had WT-like
283 function scores; and 3/4 ClinVar pathogenic/likely pathogenic variants and 16/19 presumed
284 pathogenic variants had deleterious function scores (Figures 6D and 6E). The predictive
285 performance of MAVE scores was tested by generating receiver operator characteristic (ROC)
286 curves. The area under the ROC curve was 0.90 for function scores and 0.70 for trafficking
287 scores (Figure 6F). Function scores correlated well with several previously validated
288 computational and evolutionary metrics of variant effect (Figure S11). The predictive
289 performance of function scores was comparable to these metrics (Figure S10B). We note that
290 while computational metrics perform well for *KCNE1* variants, our MAVE data are derived from
291 direct *in vitro* data, and thus provide orthogonal information. These trends were weaker for
292 trafficking scores (Figures S12 and S13).

293 We calibrated our assay with presumed pathogenic and benign variants, following the
294 approach recommended by the ClinGen Sequence Variant Interpretation working group.¹⁶ We
295 used the function scores for calibration because of their better correlation with clinical
296 outcomes and other metrics of disease risk. Using the ClinVar only dataset, the functional assay
297 achieved a likelihood ratio of pathogenicity (termed "OddsPath") of 13.0 for pathogenic
298 (PS3_moderate) and 0.253 for benign (BS3_supporting). Using the expanded set of presumed
299 benign and pathogenic variants, the functional assay achieved an OddsPath of 14.3 for
300 pathogenic (PS3_moderate) and 0.168 for benign (BS3_moderate).

301

302 **Discussion**

303 A majority of variants in clinically relevant genes, including *KCNE1*, are VUS, and
304 resolving the clinical significance of VUS at scale has been a major challenge in genomic
305 medicine.¹¹ High-throughput functional data can be deployed to reclassify as many as 89% of
306 known VUS in clinically actionable genes.¹⁵ Loss-of-function *KCNE1* variants cause type 5 long
307 QT syndrome (LQT5) via two major mechanisms: reduced cell surface expression and/or
308 defective gating (activation of the I_{Ks} complex).³² Our study ascertains trafficking and
309 electrophysiology properties to better understand the disease risk of nearly all possible *KCNE1*
310 variants. Furthermore, our dataset provides functional scores for 871 of the 924 *KCNE1* variants
311 accessible by a single SNV; each variant, if compatible with life, is estimated to exist in
312 approximately 50 humans currently alive.¹⁴ Our comprehensive datasets also reveal new
313 biology not apparent from previous smaller-scale mutational studies.

314

315 ***Insights from trafficking scores***

316 We identified 470 loss-of-trafficking and 310 gain-of-trafficking missense variants,
317 including a stretch of super-trafficking N-terminal cysteine variants. We hypothesize that these
318 residues may increase cell surface expression by forming intermolecular disulfide bonds with
319 other proteins (e.g., KCNE1 or KCNQ1). We tested this hypothesis by conducting a MAVE of cell
320 surface expression in the absence of KCNQ1, but this dataset may be influenced by other low-
321 abundance binding partners of KCNE1 endogenous to HEK293T cells. Nevertheless, the result
322 clearly implicated loss of N-glycosylation at position 26, but less so at position 5, as increasing
323 cell surface expression in the presence of KCNQ1. The cell surface abundance of nonsense
324 variants in our data also highlights that the latter half of the protein (residue 56-129) is

325 dispensable for cell surface trafficking. This residue marks the beginning of the FTL domain,
326 important for electrophysiological modulation of the I_{Ks} channel,^{33,34} and corresponds to a
327 previously reported kink in the transmembrane domain.^{35,36}

328

329 ***Insights from function scores***

330 We developed a novel selection assay that used a gain-of-function KCNQ1 variant
331 (S140G) to identify loss-of-function KCNE1 variants. With the assay, we identified 588 loss-of-
332 function variants, of which 433 (73.7%) had normal cell surface expression. We refer to these as
333 “gating” variants, as proper K⁺ flux through the I_{Ks} channel is likely disrupted. The predominance
334 of pathogenic gating variants is in contrast to other potassium channel disease genes, such as
335 KCNH2; 88% of 193 studied KCNH2 loss-of-function variants disrupt cell surface expression.³⁷
336 The high proportion of gating variants is likely explained by KCNE1’s primary function as a
337 KCNQ1-modifying subunit to modulate the I_{Ks} complex. The gating variants identified in our
338 data include well-studied variants like D76N and W87R²² and novel variants in the
339 transmembrane-proximal cytosolic domain that interact with KCNQ1 and calmodulin. We also
340 identified gating variants predicted to interact with KCNQ1 that otherwise increase KCNE1 cell
341 surface expression. These variants likely do not disrupt intermolecular binding within the I_{Ks}
342 channel complex but are rather involved in the physical modulation of KCNQ1 with appropriate
343 electrochemical stimuli.

344 Our work defines three classes of nonsense variants based on residue location: #1-55
345 that disrupt cell surface expression, #56-104 traffic to the cell surface but do not function, and
346 #105-128 have near-normal trafficking and function.³⁸ While D85N (rs1805128; AF 0.14%-2.54%

347 in gnomAD) is associated with QT prolongation and fatal arrhythmias in the presence of drugs
348 and other environmental factors,³⁹ the variant is too common to cause long QT syndrome in
349 isolation. The WT-like MAVE score estimates are concordant with this observation (trafficking
350 score: 0.82-1.00; functional score: 0.79-1.02).

351

352 ***Structural implications of MAVE data***

353 Although there is no solved cryo-EM structure of the KCNQ1-KCNE1-calmodulin
354 complex, we used AlphaFold2 and homology modeling to construct a structural model of the I_{Ks}
355 complex. In our MAVE datasets, hydrophilic variants in the hydrophobic transmembrane core
356 (including previously studied variants like L51H)²² disrupt function by affecting cell surface
357 expression. We also identify a 26 amino acid membrane-proximal cytosolic region (residues 61-
358 87) that comprises essential elements for I_{Ks} complex function: KCNQ1-binding and calmodulin-
359 binding regions, and a structured linker connecting the two. Variants in this region likely disrupt
360 hydrophobic and polar interactions and pi-stacking with the corresponding residues of KCNQ1
361 and calmodulin respectively. Accordingly, the region is highly constrained in the function, but
362 not trafficking, assay. With increasing confidence in and accuracy of AI-generated structural
363 models, the resolution and interpretation of MAVE-based structure-function relationships will
364 likely improve.

365

366 ***Clinical Associations of deleterious KCNE1 variants***

367 Our dataset also highlights the strength of association between *KCNE1* loss-of-function
368 variants and QT prolongation. In 2020, the ClinGen Channelopathy Working Group assessed

369 *KCNE1* as having only limited evidence for association with congenital type 5 long QT syndrome
370 (LQT5) and strong evidence for association with acquired long QT syndrome.⁴⁰ Since then,
371 several papers have further described the LQT5 risk of *KCNE1* variants. Roberts *et al.*¹ reported
372 in a multi-center review of LQT5 that *KCNE1* variants are a low penetrance cause of congenital
373 long QT syndrome. Our group has previously shown that carriers of pathogenic/likely
374 pathogenic *KCNE1* variants in the electronic MEdical Records and GEnomics (eMERGE)
375 sequencing study had longer QT intervals and higher odds of arrhythmia diagnoses and
376 phenotypes.⁴¹ However, these variants conferred a lower risk than P/LP variants in *KCNQ1* or
377 *KCNH2* (LQT1 and LQT2). The QT prolonging effects of deleterious *KCNE1* variants has also been
378 established in both the TOPMed and UK Biobank cohorts, with effect sizes up to 15-20 ms.⁴²
379 Thus, *KCNE1* loss-of-function variants appear to contribute to modest increases in baseline QT
380 interval.

381 The presence of a *KCNE1* deleterious variant may not be sufficient for development of
382 the congenital LQT5 phenotype. For the QT interval to rise above a high-risk threshold, LQT5-
383 associated variant carriers may require additional genetic or environmental insults, such drug
384 exposure.¹ Based on the strong correlation between MAVE scores and functional and clinical
385 outcomes, variants identified as functionally deleterious in this study likely predispose carriers
386 to LQT5.

387

388 ***MAVE data can supplement ACMG criteria***

389 Both our trafficking and function assays had excellent separation between early
390 nonsense and synonymous variants, high concordance among replicates, and strong

391 correlations with previous measurements of cell surface trafficking or patch clamp function. In
392 addition, the function MAVE dataset correlates well with patient and population cohorts, using
393 controls curated from ClinVar, literature reports, and gnomAD. Another advantage of the MAVE
394 approach is the uniformity and replication of the platform used to analyze variants, unlike
395 literature reports derived from multiple individual laboratories with low concordance.⁴³
396 Because of this heterogeneity, data from literature reports cannot accurately contribute to
397 ClinGen guidelines for interpreting *in vitro* functional datasets.¹⁶ The small number of
398 discordant variants between our assay and the literature might represent a failure of our assay
399 or of previous reports. Based on the ClinGen guidelines, function scores can be implemented at
400 the moderate level for both PS3 and BS3 criteria to aid in variant interpretation. However, given
401 the higher clinical burden of false negatives, we recommend using our scores conservatively to
402 apply BS3 at the supporting level. This work adds to the growing set of arrhythmia genes
403 previously assayed by multiplexed assays for either the full protein (KCNJ2, calmodulin)^{44,45} or a
404 portion of the protein (SCN5A, KCNH2).^{32,46,47}

405

406 **Limitations**

407 The MAVE function assay was not well-powered to detect gain-of-function variants. The
408 scores were generated in a heterologous system that may not fully model the behavior of the
409 I_{Ks} channel in a cardiomyocyte. Additionally, we did not model several known behaviors of the
410 I_{Ks} channel, such as regulation by PIP₂ or adrenergic stimulation. We also did not measure
411 dominant negative properties of the channel, demonstrated for some KCNE1 variants including

412 D76N.⁴⁸ HEK293T cells endogenously express non-KCNQ1 binding partners of KCNE1 that might
413 confound trends when assessing the trafficking of KCNE1, especially in the absence of KCNQ1.

414 While variants with the lowest trafficking scores uniformly had loss-of-function scores,
415 some partial loss-of-trafficking variants had non-deleterious function scores (Figure 4D). This
416 result may reflect the flexible stoichiometry of the channel. KCNE1 can bind to KCNQ1 in a 1:4
417 to 4:4 conformation.⁴⁹ Since KCNE1 is highly expressed in our assays, cells expressing partial
418 loss-of-trafficking variants may bind to KCNQ1 in higher proportions to activate KCNQ1 and
419 yield some I_{Ks} function.

420 Although KCNE1's major role in the cardiac action potential is through its role in I_{Ks} ,
421 KCNE1 has also been reported to interact with other proteins including KCNH2⁵⁰ and
422 TMEM16A, a cardiac chloride channel.⁵¹ These interactions might influence arrhythmia risk that
423 is not captured by the I_{Ks} assay performed in this study. For example, previously discussed
424 variant D85N has been reported to cause a partial loss-of-function of KCNH2,⁵² which may
425 explain its influence on the QT interval. An extension of this work would be to investigate the
426 influence of comprehensive KCNE1 variant libraries on other protein complexes.

427

428 **Conclusions**

429 We comprehensively ascertained variant function in an important arrhythmia gene,
430 KCNE1. We identified 470 variants that affect KCNE1 trafficking and 588 variants that alter
431 function. Our work highlights new biology of the I_{Ks} channel and can be implemented in the
432 ACMG/AMP scheme to classify variants.

433

435 **Declarations**

436 ***Ethics approval and consent to participate***

437 Not applicable.

438

439 ***Consent for publication***

440 Not applicable.

441

442 ***Availability of data and materials***

443 The three MAVE datasets supporting the conclusions of this article are available in Additional
444 File 2 and will be deposited in MaveDB⁵³ upon publication. Illumina sequence data will be
445 archived in the Short Read Archive upon publication. Code to analyze MAVE data and re-create
446 figures is available at https://github.com/GlazerLab/KCNE1_DMS.

447

448 ***Competing interests***

449 The authors declare that they have no competing interests.

450

451 ***Funding***

452 This research was funded by R00 HG010904 (AMG), R01 HL149826 (DMR), R01 HL164675
453 (DMR) and RM1 HG010461 (DMF). AM received support from the American Heart Association
454 (2OPRE35180088) and the Vanderbilt Medical Scientist Training Program (T32GM007347). Flow
455 cytometry experiments were performed in the VUMC Flow Cytometry Shared Resource, which

456 is supported by the Vanderbilt Ingram Cancer Center (P30 CA68485) and the Vanderbilt
457 Digestive Disease Research Center (DK058404).

458

459 ***Author Contributions***

460 AM, DMR, and AG designed the research and wrote the manuscript. AM, MC, BL, TY, DJB, MLH,
461 JS, AEC, and AMG performed the research. AM, MC, BL, TY, DJB, JS, DMR, and AMG analyzed
462 the data. JAC, KAM, and DMF contributed essential resources and reagents. All authors
463 reviewed and approved the manuscript.

464

465 ***Acknowledgements***

466 We thank Fritz Roth, Jochen Weile, Bjorn Knollmann, David Samuels, the CardioVar consortium,
467 and members of the Vanderbilt Center for Arrhythmia and Therapeutics for helpful discussions.
468 We thank Kara Skorge, Laura Short, Marcia Blair, and Lynn Hall for cloning assistance and the
469 Vanderbilt VANTAGE sequencing core for performing Illumina sequencing.

470

471 ***Author's Twitter handles***

472 @ayeshamyar (AM), @capra_lab (JAC), @kmatreyek (KAM), @dougowler42 (DMF),
473 @rodendm (DMR), and @amglazer (AMG)

474

475 **Methods**

476 ***Overview of multiplexed assays of KCNE1 variant effects***

477 An HA epitope tag was cloned into the extracellular region of *KCNE1*. Saturation
478 mutagenesis was used to create a plasmid library of 2,592 distinct single amino acid *KCNE1*
479 variants (95.7% of total possible variants). Each plasmid was associated with a random 18-base
480 barcode and the plasmid library was “subassembled”, i.e., deep sequenced to connect each
481 barcode to its corresponding *KCNE1* variant. To express one *KCNE1*-HA variant per cell, the
482 library was integrated into Human Embryonic Kidney (HEK) 293T cells engineered to include a
483 “landing pad.”¹⁸ To determine cell surface expression, *KCNE1*-HA variants were expressed with
484 or without WT *KCNQ1* and the cell pool was stained with an anti-HA antibody. Cells were sorted
485 into 4 bins based on the level of cell surface labeling, and each bin was deep sequenced to
486 quantify variants. To determine channel function, *KCNE1*-HA variants were expressed with a
487 gain-of-function *KCNQ1* variant for 20 days to deplete cells with normally functioning I_{Ks}
488 channels. The cell pool was deep sequenced at day 0, 8 and 20 to quantify variants (Figure S1).

489

490 ***Cloning a novel KCNE1 HA tag***

491 We used *KCNE1* (NCBI Reference Sequence NM_001127670.4) with the G allele at residue 38
492 (p.S38G, c.112A>G, rs1805127), as this variant allele is more common globally (65.8% allele
493 frequency [AF] across all ancestral populations in gnomAD; range 57.4%-71.3%).⁵⁴ An HA
494 epitope (5'-TACCCCTACGATGTACCAGATTATGCG-3') was cloned between residues 34 and 35
495 with primers ag424 and ag425 using inverse PCR with Q5 polymerase (New England Biolabs,
496 NEB).²³ The sequences of all primers used in this study are presented in Table S2. The resulting
497 gene, *KCNE1*-HA, was subcloned into the pIRE2-dsRED2 plasmid using PCR with ag409 and
498 ag410 and NotI restriction digestion (NEB) to create *KCNE1*-HA:pIRE2:dsRED2. All plasmid

499 sequences were verified with Sanger sequencing. Using NotI restriction digestion, the *KCNE1-*
500 HA gene was moved to an AttB plasmid containing pIRES:mCherry:BlastR to create p*KCNE1-*
501 HA:IRES:mCherry:BlastR. We also used a compact (<4kb) promoterless plasmid for single-
502 variant mutagenesis.⁴⁶ Maps of key plasmids used in this study are shown in Figure S14A.

503

504 ***Generation of HEK293T lines stably expressing KCNQ1 or KCNQ1-S140G***

505 The experiments were conducted in either previously published Bxb1-mediated landing pad
506 HEK293T (LP) cells,¹⁸ or LP cells genetically engineered to express *KCNQ1* (WT or S140G). LP
507 cells contain an AttP integration “landing pad,” Blue Fluorescent Protein (BFP), and iCasp9
508 caspase downstream of a doxycycline-induced promoter.¹⁸ The AttB:mCherry:BlastR plasmid
509 integrates into the AttP landing pad. Prior to integration, the promoter drives BFP and iCasp9
510 expression. After integration, the promoter drives expression of mCherry and blasticidin
511 resistance genes instead. Cells with a successful plasmid integration event are blasticidin
512 resistant, express mCherry and lack iCasp9, which can be used to select for recombined cells.

513 Genetically engineered LP cells expressing *KCNQ1* (WT or S140G) were generated as below.

514

515 Since the plasmids use NotI restriction digestion for subcloning, we removed an intra-cDNA
516 NotI restriction enzyme site, by introducing a synonymous mutation (c.246G>T), into WT
517 *KCNQ1* cDNA (NM_000218.3) using QuikChange mutagenesis (Agilent). The *KCNQ1* gain-of-
518 function variant (p.S140G, c.418A>G, rs120074192) was also generated by QuikChange
519 mutagenesis. *KCNQ1* S140G biases I_{Ks} channels to the open state^{29,31} at lower membrane

520 potentials (including the resting potential of HEK293T cells, approximately -25 mV)²⁸ and leads
521 to increased cellular K⁺ efflux.⁵⁵

522

523 To construct a cell line with constitutive *KCNQ1* expression, *KCNQ1* (WT or p.S140G) was cloned
524 into a Sleeping Beauty transposon system, pSBbi-GN (a gift from Eric Kowarz, Addgene#
525 60517),⁵⁶ using Sfil restriction digestion (NEB) to create pSBbi-GN::KCNQ1. This plasmid
526 expresses *KCNQ1* and *EGFP* via constitutively active bidirectional promoters. The plasmid was
527 randomly integrated into a non-landing pad locus in the LP cells with the Sleeping Beauty
528 transposase as follows. Cells were cultured at 37° at 5% CO₂ in HEK media: 10% FBS (Corning),
529 1% non-essential amino acids (Corning), 1% penicillin/streptomycin (Corning) in DMEM
530 (Thermo). On day 0, pSBbi-GN::KCNQ1 was transfected into the LP cell line along with a plasmid
531 expressing the Sleeping Beauty transposase, pCMV(CAT)T7-SB100 (a gift from Zsuzsanna Izsvák,
532 Addgene #34879),⁵⁷ using FuGENE6 (Promega) in a 1:3 ratio with DMEM. On day 6, the cells
533 were exposed to HEK media with 1 µg/mL doxycycline (Sigma) to induce expression of the
534 BFP/iCasp9 from the landing pad. The cells were sorted with a BD FACSAria IIIU (BD
535 Biosciences), using a 100 µm nozzle for cells with high levels of BFP and high levels of GFP
536 (Figure S14B) into HEK media on amine-coated plates (Corning). Single-cell colonies were grown
537 in HEK media, with the addition of 1 µg/mL doxycycline 48 hours before being screened on a BD
538 LSRII Fortessa SORP (BD Biosciences) to identify colonies with high rates of both landing pad (*BFP*)
539 and *KCNQ1* (*GFP*) expression (Figure S14C). Two distinct colonies with high blue and green
540 fluorescence were expanded for further experiments. The landing pad cell line expressing WT

541 KCNQ1 is referred to as LP-KCNQ1 and the cell line expressing KCNQ1 S140G is referred to as
542 LP-KCNQ1-S140G.

543

544 For transient transfection experiments, plasmids that constitutively expressed *KCNE1* or *KCNQ1*
545 were cloned using NotI restriction digestion into pIRES2:EGFP or pIRES2:dsRED2 to create all
546 four combinations: p*KCNE1*:IRES:EGFP, p*KCNE1*:IRES:dsRED2, p*KCNQ1*:IRES:EGFP, and
547 p*KCNQ1*:IRES:dsRED2 (see Supplemental Methods for more details).

548

549 ***KCNE1 library creation***

550 Each of the 129 *KCNE1* residues was comprehensively mutated using inverse PCR on the
551 compact template plasmid.^{23,46} For each mutagenesis reaction, the forward primers contained a
552 5' degenerate NNK sequence for each codon to introduce all 20 sense amino acid variants and 1
553 nonsense variant at each site. The 129 PCR reactions were pooled, PCR-purified (QIAGEN),
554 phosphorylated with T4 PNK (NEB), and self-ligated using T4 ligase (NEB). The pooled product
555 was re-PCR-purified and electroporated into ElectroMAX DH10B Cells (ThermoFisher) using a
556 Gene Pulser Electroporator (Bio-Rad; 2.0 kV, 25 µF, 200 Ω). Serial dilutions of the
557 electroporated cells were plated on Ampicillin plates to determine transformation efficiency.
558 The library was purified using a MaxiPrep kit (Qiagen) and subcloned into a promoterless AttB
559 pIRES:mCherry-BlastR^{18,46} plasmid using restriction digestion with AatII and AflII (NEB). The
560 library was then re-electroporated and purified as above.

561 For quantification, each variant construct was tagged with a random 18mer barcode to
562 the library plasmid. The barcode was generated using ag289 (spacer-BsiWI-AfII-N18-AatII-XbaI-

563 spacer) and ag290 (reverse complement of the 3' end of ag289). The two primers were
564 annealed by incubating at 95° for 3 minutes and cooling by 1°/10 s. The annealed primers were
565 extended to fully double stranded DNA using Klenow polymerase (NEB). The barcode was
566 purified by phenol-chloroform extraction, digested with BsiWI and XbaI (Thermo Fisher), and
567 re-purified by phenol-chloroform extraction. The resulting DNA fragment was ligated into the
568 *KCNE1*-HA plasmid library. The plasmid library was deep sequenced to link each barcode to its
569 associated variant (see Supplemental Methods). A map of the final barcoded plasmid library
570 (*pKCNE1*-HA library:*pIRES*:dsRed:BlastR) is provided in Figure S3A.

571

572 ***Integration of library into landing pad cells***

573 LP, LP-KCNQ1, or LP-KCNQ1-S140G cells were cultured in 10 cm dishes in HEK media until
574 approximately 60% confluent. Cells were then transfected with 25 µg of *pKCNE1*-HA
575 library:*IRES*:dsRed:BlastR and 5µg of site-specific recombinase, pCAG-NLS-HA-Bxb1 (a gift from
576 Paweł Pelczar, Addgene #51271)⁵⁸ using Lipofectamine 2000 (Thermo Fisher) in a 1:2 ratio.¹⁸ 6-
577 8 hours after transfection, the cells were fed fresh media. The following day, cells were
578 passaged using Accutase (Sigma) into two 10 cm dishes and fed media supplemented with 1
579 µg/mL doxycycline (Sigma) to induce expression of the landing pad. With successful integration
580 of a single AttB-containing plasmid, the landing pad expresses only one *KCNE1*-HA variant,
581 mCherry, and BlastR. 24 hours later, cells were singularized in place using 1 mL Accutase,
582 quenched with 10 mL selection media (HEK media as above with 1 µg/mL doxycycline, 100
583 µg/mL blasticidin (Sigma), and 10nM AP1903 (MedChemExpress)). Addition of blasticidin and
584 AP1903 selected for successfully integrated cells that expressed *KCNE1*-HA

585 library:pIRES:mCherry:BlastR and against non-integrated cells that continued to express
586 BFP/iCasp9 caspase. Cells were grown in selection media for 8 days post-transfection. For the
587 LP-KCNQ1-S140G line, cells with successful integration were enriched in HEK selection media
588 containing a high concentration (500 nM) of the HMR 1556 (Tocris), a specific I_{Ks} blocker with
589 an IC_{50} of 10.5 nM.⁵⁹

590

591 **Trafficking assay**

592 We measured cell surface trafficking of the KCNE1-HA library in the presence and absence of
593 KCNQ1, using LP-KCNQ1 and LP cells, respectively. Each experiment was performed in triplicate
594 (three independently transfected, stained, sorted, and sequenced replicates).

595 To stain KCNE1-HA at the cell surface, day 8 post-selection, cells were dissociated using
596 Accutase and quenched with HEK selection media. For any subsequent cellular suspension, cells
597 were centrifuged for 5 minutes at 300 g and suspended in the new solution. The cells were
598 washed with block solution (1% FBS +25 mM HEPES pH 7.0 [Sigma] in PBS without Ca^{2+}/Mg^{2+}).
599 The cells were then stained with 1:500 anti-HA AF647 conjugated antibody (Cell Signaling
600 #3444) in block solution for 45 minutes at room temperature in the dark and washed three
601 times. Stained cells were resuspended in block solution at a concentration of 4-6 million
602 cells/mL for sorting. Two trafficking experimental replicates were performed with cells in
603 suspension as described above. One replicate was stained while cells were adhered on the dish
604 (see Supplemental Methods).

605 Stained cells were FACS sorted on the BD FACSAria III (BD Biosciences) using a 100 μ m
606 nozzle. Compensation was performed using cells expressing single fluorophores or AF647

607 compensation beads (Thermo Fisher). Single cells were identified based on forward and side
608 scatter signals. BFP⁻/mCherry⁺ single cells (with and without GFP for *KCNE1* with and without
609 *KCNQ1* experiments, respectively) were divided into 4 groups of approximately equal size based
610 on AF647 labeling (Figure S15). At least 800,000 cells per group were sorted and replated onto
611 amine-coated plates containing HEK media. Cells were expanded and genomic DNA was
612 extracted from each group with the Quick-DNA midiprep kit (Zymo). Q5 polymerase was used
613 to amplify the barcodes from gDNA with 20 cycles of amplification using Illumina-compatible
614 primer pairs (Table S2), and the barcodes were sequenced on the Illumina NovaSeq PE150 with
615 at least 25 million reads per sample. Normalized cell surface trafficking scores were calculated
616 from a weighted average of barcode counts from these samples (see Supplemental Methods for
617 details).

618

619 ***Cell fitness assay***

620 The cell fitness assay was validated by 1:1 competition experiments on control variants (see
621 Supplemental Methods for details) and then conducted on the entire library. The
622 comprehensive library was integrated into the landing pad of cells as described above. Fitness
623 of cells expressing *KCNE1*-HA variants in the library was measured in LP-KCNQ1-S140G in three
624 independent replicates. 8 days after successful plasmid integration, termed Day 0 in
625 subsequent analyses, cells were washed with selection media to remove HMR 1556, and a
626 subset of cells harvested for gDNA extraction. Cells were passaged as needed. Additional
627 samples were harvested for gDNA extraction on Day 8 and Day 20. Genomic DNA from these

628 three time points (Days 0, 8 and 20) was isolated. Barcode pools were amplified and sequenced
629 using the Illumina NovaSeq as described above.

630

631 ***Population-level analyses***

632 The data for putative controls were obtained from gnomAD v.2.1.1 (exomes and genomes,
633 accessed October 2022).⁵⁴ Variant annotations were obtained from the ClinVar database
634 (accessed October 2022).¹³ In addition, we performed a literature review that consisted of a
635 PubMed search (on November 30, 2022) for “KCNE1.” The resulting 929 manuscript titles and
636 abstracts were manually reviewed to collate published patch clamp electrophysiology and
637 patient data (Additional File 1, see Supplemental Methods for more details). Variants in at least
638 1 patient with LQT5 (Romano-Ward or one allele of JLNS) and an AF < 2.5x10⁻⁵ across all
639 ancestries in gnomAD were classified as putative LQT5-associated variants. Similarly, the 2
640 variants previously seen in cases with atrial fibrillation, G25V and G60D, also had allele
641 frequencies < 2.5x10⁻⁵, and thus were classified as putative atrial fibrillation-associated variants.
642 Putative benign variants had an estimated penetrance of < 10% ($\frac{\#}{\# + \#}$) and had an allele
643 frequency of > 3x10⁻⁵ in gnomAD. Only 1 variant (G55S) with an allele frequency of > 3x10⁻⁵ had
644 a penetrance of > 10% and was excluded.

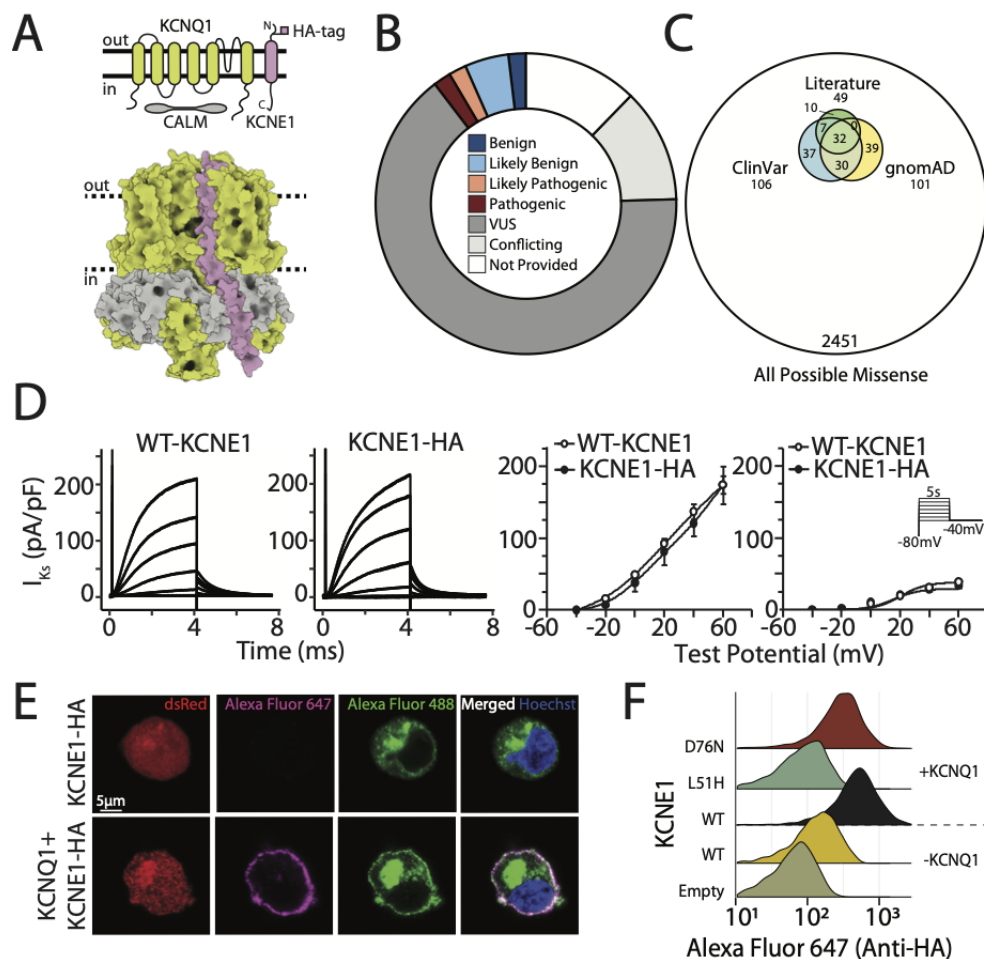
645

646 ***ACMG Assay Calibration***

647 Missense variants classified in ClinVar as pathogenic/likely pathogenic or in our curated list of
648 putative LQT5 variants were classified as “presumed cases.” Missense variants classified as
649 benign/likely benign in ClinVar or in our curated list of putative normal variants were classified

650 as “presumed controls”. Variants with score estimates (mean and 95% confidence interval)
651 below the 2.5th percentile or above the 97.5th percentile of the synonymous distribution were
652 defined as loss-of-function and gain-of-function respectively. Variants with score estimates
653 within the cutoffs were classified as “functionally WT-like.” Missense variants score estimates
654 that overlapped the cutoffs were classified as “indeterminate.” Only one variant (Y107R) had a
655 function score estimate higher than the 97.5th percentile cutoff. To determine the strength of
656 evidence at which MAVE scores could be used as evidence for the ACMG functional assay
657 criteria (PS3/BS3), the assay OddsPath was calculated using previously described methods.¹⁶

658

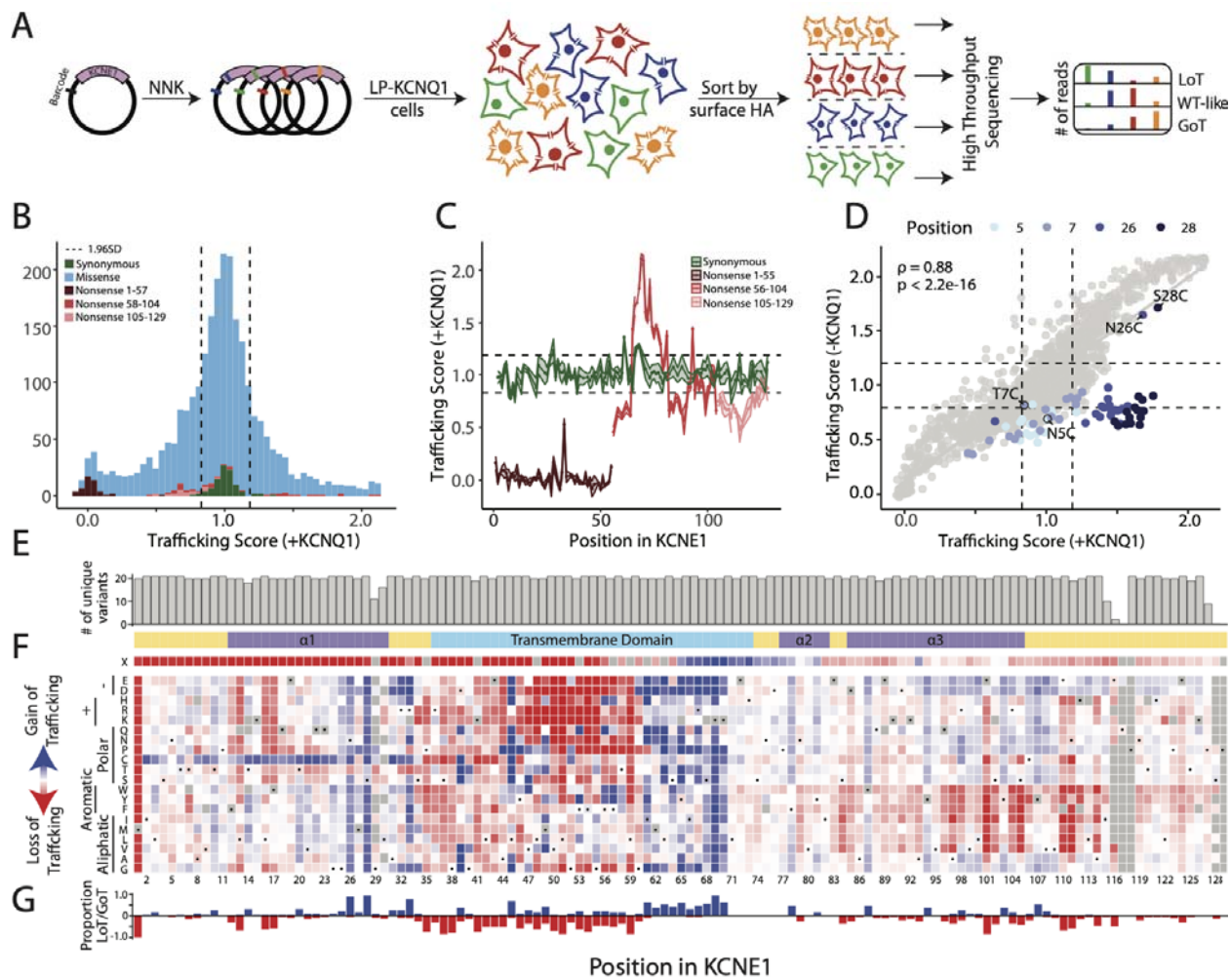


659

660 **Figure 1: Overview of the I_{K_s} channel and a novel location for the HA epitope**

661 A) The I_{K_s} channel complex is formed by KCNE1 (pink), KCNQ1 (green), and calmodulin (gray);
662 top: schematic, and bottom: three-dimensional structure). The HA tag in KCNE1 (cloned
663 between residues 34 and 35) is labeled. B) Most of the 106 missense KCNE1 variant
664 classifications in the ClinVar database are VUS or conflicting (Figure style adapted from Starita
665 et al., 2017). C) Variants reported in ClinVar, gnomAD, and previous studies comprise a small
666 portion of all possible KCNE1 missense variants. D) The HA tag did not disrupt I_{K_s} (left:
667 representative traces, inset: voltage protocol, and right: quantification of peak and tail current;
668 n=4 cells/condition). E) An HA tag was used to visualize KCNE1. Live HEK293T cells were stained
669 with an Alexa Fluor 647-conjugated anti-HA antibody to detect surface KCNE1, then fixed,
670 permeabilized, and stained with an Alexa Fluor 488-conjugated anti-HA antibody to detect total
671 KCNE1. dsRed is the KCNQ1 and KCNE1 transfection marker. Cells expressing only KCNE1-HA
672 showed minimal surface labeling in the absence of KCNQ1 (top). Cells expressing KCNE1-HA and
673 KCNQ1 had normal cell surface expression (bottom). F) Live cells stained for extracellular
674 KCNE1-HA had minimal but detectable labeling in the absence of KCNQ1, but 6.1-fold higher
675 labeling in the presence of KCNQ1. Known trafficking-null variant (L51H) had minimal cell
676 surface expression, but a known gating variant (D76N) had near-wild type cell surface
677 expression.

678

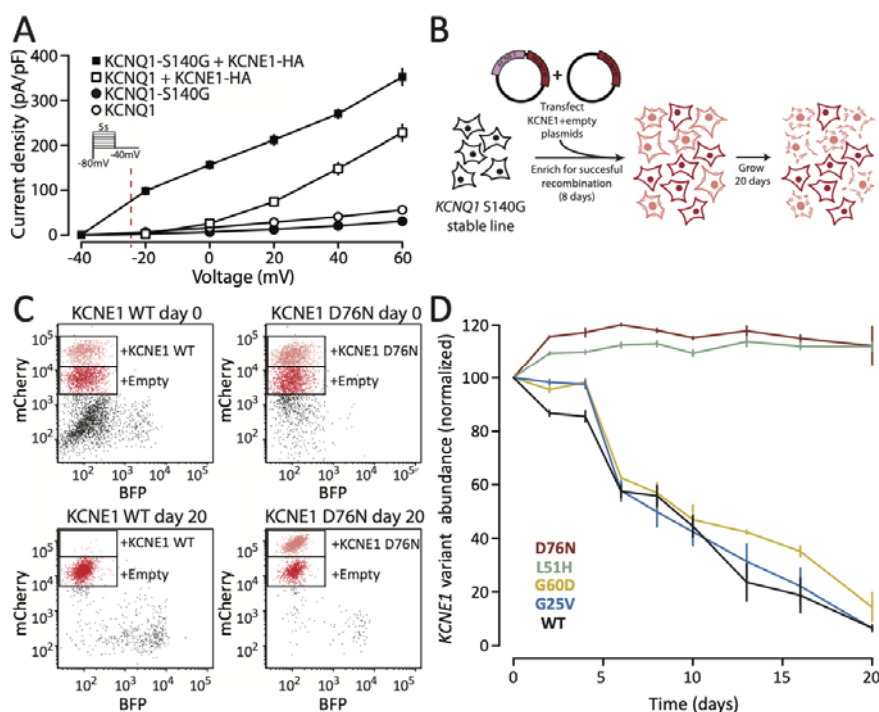


679

680 **Figure 2: Multiplexed assay of KCNE1 cell surface expression**

681 A) To conduct the cell surface expression multiplexed assay of *KCNE1*, a comprehensively
682 mutated barcoded plasmid pool was integrated into the LP-KCNQ1 cell line. Cells were stained
683 and sorted by surface *KCNE1* levels and deep sequenced. B) Histogram of normalized trafficking
684 scores by functional class showed a unimodal distribution of missense variant scores centered
685 at the median of synonymous variant scores. A smaller peak at the median of early nonsense
686 variant scores and a tail of super-trafficking variant scores was also seen (Dotted lines: mean ±
687 1.96 SD for the synonymous distribution). C) Most nonsense variants (1 per residue) from
688 residues 1-55 (brown) are loss-of-trafficking but nonsense variants after residue 55 (red or pink)

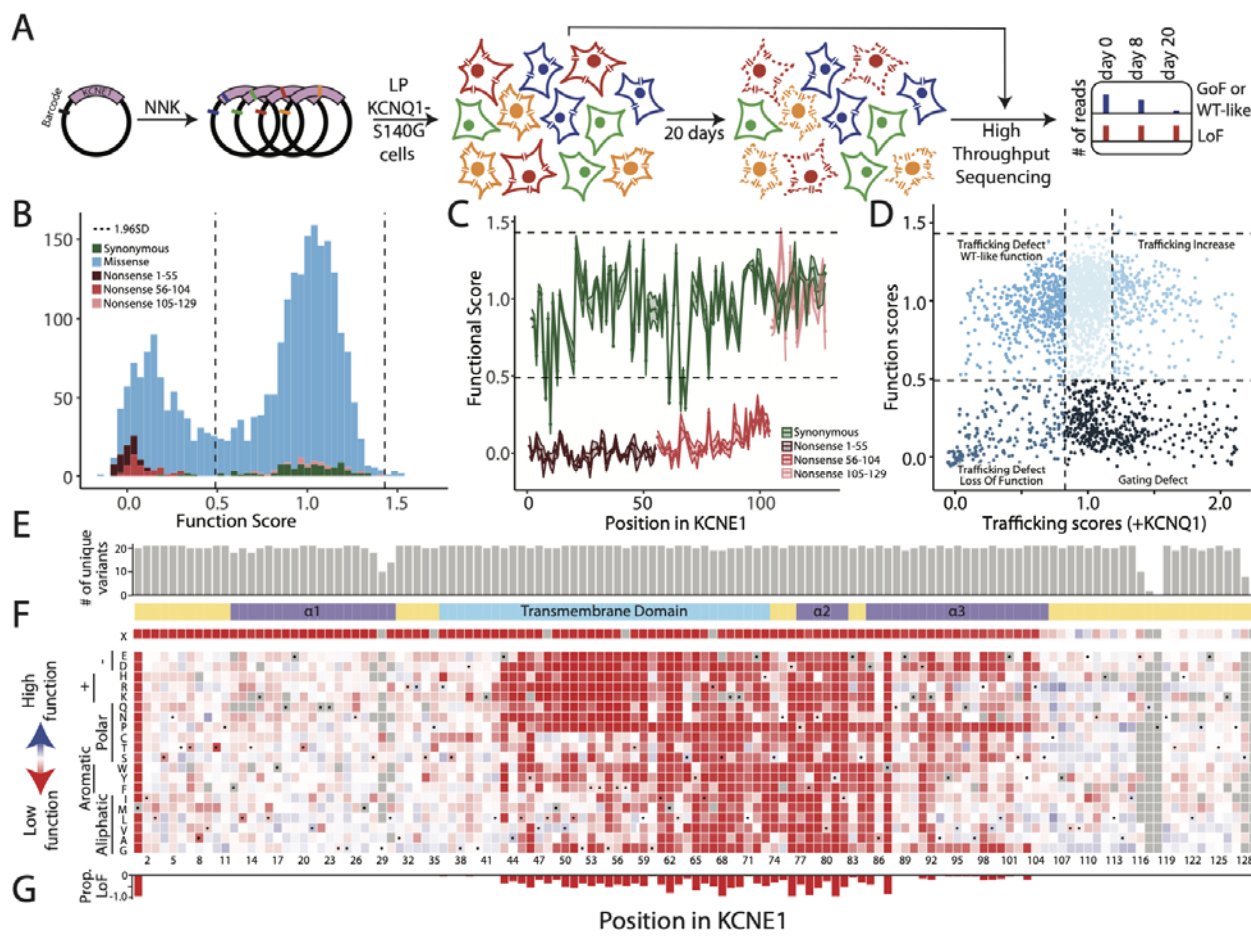
689 are gain-of-trafficking or WT-like. Synonymous variants (1 per residue) are represented in green
690 (Dotted lines: mean \pm 1.96 SD for the synonymous distribution). D) Trafficking scores in the
691 presence and absence of KCNQ1 were highly correlated with the exception of variants at
692 residues 5, 7, 26, and 28 which disrupted glycosylation sequons (highlight). Cysteine variants at
693 these sequons did not follow this trend (annotation). See Figure S5 for a full description of the
694 KCNQ1⁻ trafficking assay (Dotted lines: mean \pm 1.96 SD for the synonymous distribution). E)
695 Near complete representation of variants was scored at each position in the KCNE1 protein
696 (max = 21). F) A heatmap showing trafficking scores. Red, white, and blue indicate low, WT-like,
697 and high cell surface expression, respectively. WT amino acids are indicated at each position
698 with a dot. The colored ribbon indicates secondary structure, (purple = alpha helices, light blue
699 = transmembrane domain, yellow = unstructured regions). G) For each residue, the proportion
700 of gain-of-trafficking (GoT) and loss-of-trafficking (LoT) missense variants is displayed.



702 **Figure 3: A KCNE1 function assay using a gain-of-function KCNQ1 variant**

703 A) Voltage clamp measurements of outward potassium currents in HEK293T cells transfected
704 with various combinations of WT or S140G KCNQ1 and/or KCNE1-HA. At the resting potential of
705 HEK293T cells (~ -25 mV, dotted line), there is almost no potassium current in cells transfected
706 with KCNQ1 ± KCNE1-HA. However, the gain-of-function KCNQ1-S140G variant results in a
707 leftward shift of voltage of activation and increased current at -25 mV, only in the presence of
708 KCNE1. B) Experiment to validate KCNE1 selection assay using LP-KCNQ1-S140G cells
709 transfected with 1:1 pools of KCNE1 variant and empty vector plasmids. C) Representative flow
710 cytometry measurements of cells transfected with 1:1 pools of plasmids. Cells with empty
711 vectors had reduced mCherry fluorescence allowing quantification of distinct cell populations.
712 After 20 days of selection, there was a strong depletion of cells expressing KCNE1-HA-WT but
713 not a loss-of-function variant D76N. D) Time course of relative fitness of cells expressing KCNE1
714 variants compared to cells expressing empty vectors. All values are normalized to the values at
715 day 0. Cells expressing KCNE1-HA-WT or two gain-of-function variants (G25V and G60D)
716 depleted over 20 days but cells expressing two loss-of-function variants (D76N and L51H)
717 persisted in the cell pool. Points and error bars indicate mean and standard error of three
718 replicates.

719

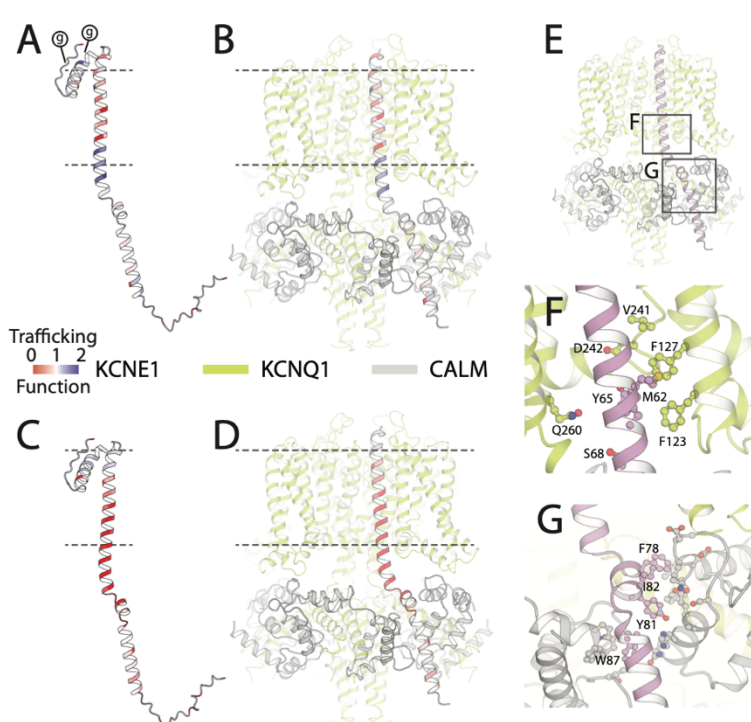


720

721 **Figure 4: Multiplexed assay of *KCNE1* function**

722 A) Schematic of multiplexed assay of *KCNE1* function. A comprehensively mutated barcoded
723 plasmid pool was integrated into LP-KCNQ1-S140G cells. Cells were grown for 20 days and cell
724 pools at 0 days, 8 days, and 20 days were deep sequenced. B) Histogram of normalized
725 functional scores by functional class showed a bimodal distribution of missense variants
726 (Dotted lines: mean \pm 1.96 SD for the synonymous distribution). C) Nonsense variants (1 per
727 residue) up to residue 104 are functionally deleterious (brown and red), including residues 56-
728 104 that were dispensable for cell surface trafficking (red). Synonymous variants (1 per residue)
729 are represented in green (Dotted lines: mean \pm 1.96 SD for the synonymous distribution). D)
730 Relationship between trafficking and function scores for missense variants showed that most

731 deleterious variants disrupt gating (Dotted lines: mean \pm 1.96 SD for the synonymous
732 distribution). E) Near complete representation of missense variants was scored at each position
733 in KCNE1 (max = 21). F) KCNE1 function score heatmap. Red, white, and blue indicate loss-of-
734 function, normal function, and gain-of-function, respectively. WT amino acids are indicated at
735 each position with a dot. The colored ribbon indicates secondary structure as in Figure 2. G) For
736 each residue, the proportion of loss-of-function missense variants is displayed.
737

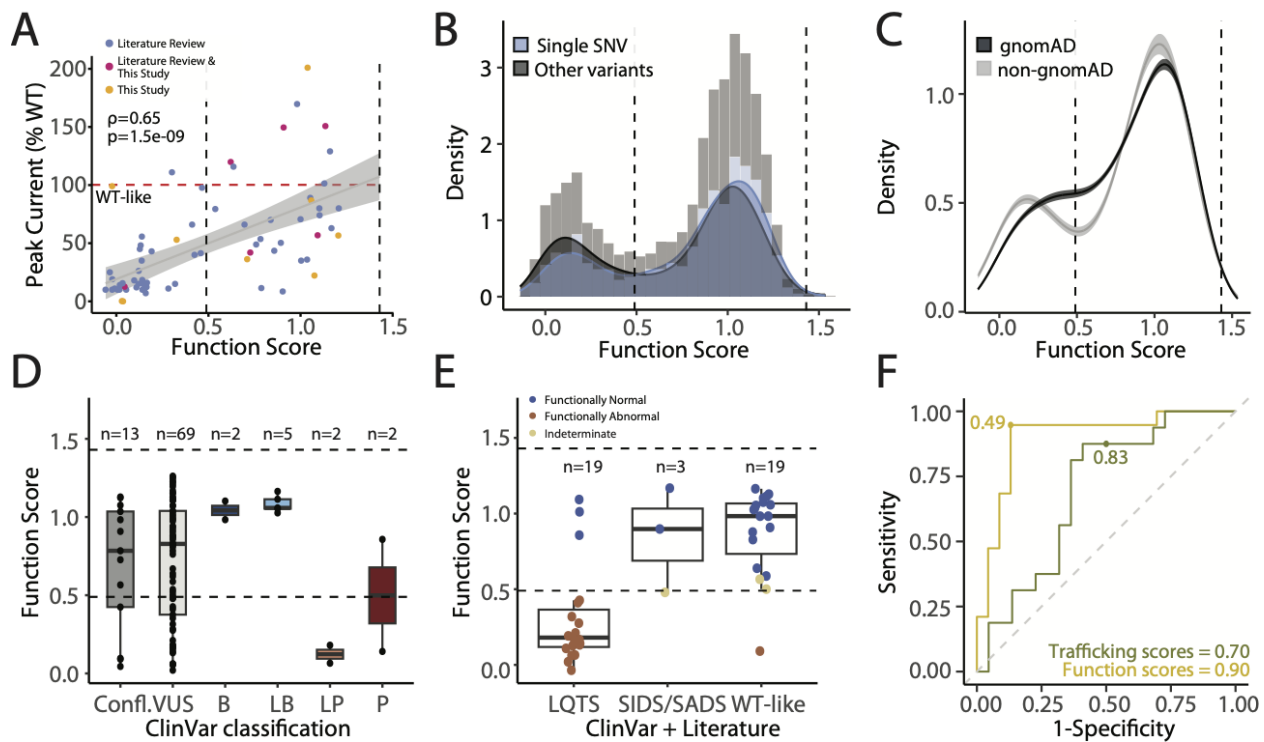


738

739 **Figure 5: Structural impact of variant effects**

740 A-D) KCNE1 structural model, coded by mean trafficking scores (A,B) or function scores (C,D) at
741 each residue on the same color scale as in Figures 2F and 4F (Red = loss-of-trafficking/function,
742 white = WT-like, blue = gain-of-trafficking/function). Dotted lines indicate the approximate
743 location of the plasma membrane. (g) represents glycosylation sites. Panels B and D show

744 KCNE1 in complex with KCNQ1 (green) and calmodulin (gray). E) I_{Ks} complex showing locations
745 of panels F and G. F) Constrained KCNE1 residues (pink) that make contacts with KCNQ1. KCNE1
746 residue M62 forms a hydrophobic cluster with KCNQ1 residues F123, F127 and V241, whereas
747 KCNE1 residues Y65 and S68 make polar contacts with KCNQ1 residues D242 and Q260,
748 respectively. G) Constrained KCNE1 residues (pink; F78, Y81, I82, W87) that make contacts with
749 calmodulin. Residues on calmodulin not labeled.
750



751
752 **Figure 6: Function scores correlate with *in vitro* assays and clinical outcomes**

753 A) Correlation of function scores with peak current (normalized to WT) from patch clamp
754 studies. Blue: literature review, pink: literature review and this study, yellow: this study. B)
755 Single SNV variants (blue) are less likely to have deleterious function scores compared to all
756 other variants (black; $p = 9.3 \times 10^{-6}$, Wilcoxon Test). C) Variants present in gnomad (black) were

757 more likely to have WT-like scores than variants absent from gnomAD (grey; $p=2.2\times10^{-4}$,
758 Wilcoxon Test). Mean and confidence intervals are generated by re-sampling both distributions
759 100 times. D) Function scores by ClinVar classification. E) Function scores for presumed control
760 and presumed disease-associated variants. See Additional File 1 for the literature review
761 dataset. F) Receiver operator characteristic curves evaluating prediction of variant
762 pathogenicity by function and trafficking scores. Dots indicate the deleteriousness cutoffs used
763 in this study (functional scores = 0.49, trafficking scores = 0.83). The area under the curve is
764 listed at the bottom of the panel.

765

766 **Additional files**

767 Additional File 1: Literature review of KCNE1 variants. File name: AdditionalFile_LitRev.csv

768 Additional File 2: Function and trafficking scores for KCNE1 variants. File name:
769 AdditionalFile_MAVEscores.csv

770 Additional File 3: Structure of the KCNE1/KCNQ1/calmodulin complex with mean function
771 scores at each residue overlaid on KCNE1. File name: KCNE1-AF2-full-func-score-mapped.pdb

772 Additional File 4: Structure of the KCNE1/KCNQ1/calmodulin complex with mean trafficking
773 scores at each residue overlaid on KCNE1. File name: KCNE1-AF2-full-traffick-score-mapped.pdb

774 Additional File 5: Computational scores curated for variants tested in this study. File name:
775 AdditionalFile_CompScores.csv

776

777 **References**

778 1. Roberts, J. D. *et al.* An International Multicenter Evaluation of Type 5 Long QT Syndrome: A Low

- 779 Penetrant Primary Arrhythmic Condition. *Circulation* **141**, 429–439 (2020).
- 780 2. Splawski, I., Tristani-Firouzi, M., Lehmann, M. H., Sanguinetti, M. C. & Keating, M. T. Mutations in
781 the hminK gene cause long QT syndrome and suppress IKs function. *Nat. Genet.* **17**, 338–340
782 (1997).
- 783 3. Schulze-Bahr, E. *et al.* KCNE1 mutations cause jervell and Lange-Nielsen syndrome. *Nat. Genet.* **17**,
784 267–268 (1997).
- 785 4. Splawski, I. *et al.* Spectrum of mutations in long-QT syndrome genes. KVLQT1, HERG, SCN5A,
786 KCNE1, and KCNE2. *Circulation* **102**, 1178–1185 (2000).
- 787 5. Westenskow, P., Splawski, I., Timothy, K. W., Keating, M. T. & Sanguinetti, M. C. Compound
788 mutations: a common cause of severe long-QT syndrome. *Circulation* **109**, 1834–1841 (2004).
- 789 6. Kapplinger, J. D. *et al.* Spectrum and prevalence of mutations from the first 2,500 consecutive
790 unrelated patients referred for the FAMILION long QT syndrome genetic test. *Heart Rhythm* **6**,
791 1297–1303 (2009).
- 792 7. Olesen, M. S. *et al.* Mutations in the potassium channel subunit KCNE1 are associated with early-
793 onset familial atrial fibrillation. *BMC Med. Genet.* **13**, 24 (2012).
- 794 8. Yus-Najera, E., Santana-Castro, I. & Villarroel, A. The identification and characterization of a
795 noncontinuous calmodulin-binding site in noninactivating voltage-dependent KCNQ potassium
796 channels. *J. Biol. Chem.* **277**, 28545–28553 (2002).
- 797 9. Harmer, S. C., Wilson, A. J., Aldridge, R. & Tinker, A. Mechanisms of disease pathogenesis in long
798 QT syndrome type 5. *Am. J. Physiol. Cell Physiol.* **298**, C263–73 (2010).
- 799 10. Richards, S. *et al.* Standards and guidelines for the interpretation of sequence variants: a joint
800 consensus recommendation of the American College of Medical Genetics and Genomics and the
801 Association for Molecular Pathology. *Genet. Med.* **17**, 405–424 (2015).
- 802 11. Green, E. D. *et al.* Strategic vision for improving human health at The Forefront of Genomics.

- 803 *Nature* **586**, 683–692 (2020).
- 804 12. Starita, L. M. *et al.* Variant Interpretation: Functional Assays to the Rescue. *Am. J. Hum. Genet.* **101**,
805 315–325 (2017).
- 806 13. Landrum, M. J. *et al.* ClinVar: improving access to variant interpretations and supporting evidence.
807 *Nucleic Acids Res.* **46**, D1062–D1067 (2018).
- 808 14. Weile, J. & Roth, F. P. Multiplexed assays of variant effects contribute to a growing genotype-
809 phenotype atlas. *Hum. Genet.* **137**, 665–678 (2018).
- 810 15. Fayer, S. *et al.* Closing the gap: Systematic integration of multiplexed functional data resolves
811 variants of uncertain significance in BRCA1, TP53, and PTEN. *Am. J. Hum. Genet.* **108**, 2248–2258
812 (2021).
- 813 16. Brnich, S. E. *et al.* Recommendations for application of the functional evidence PS3/BS3 criterion
814 using the ACMG/AMP sequence variant interpretation framework. *Genome Med.* **12**, 3 (2019).
- 815 17. Fowler, D. M. & Fields, S. Deep mutational scanning: a new style of protein science. *Nat. Methods*
816 **11**, 801–807 (2014).
- 817 18. Matreyek, K. A., Stephany, J. J. & Fowler, D. M. A platform for functional assessment of large
818 variant libraries in mammalian cells. *Nucleic Acids Res.* **45**, e102 (2017).
- 819 19. Wang, K. W. & Goldstein, S. A. Subunit composition of minK potassium channels. *Neuron* **14**, 1303–
820 1309 (1995).
- 821 20. Jiang, M. *et al.* Dynamic partnership between KCNQ1 and KCNE1 and influence on cardiac IKs
822 current amplitude by KCNE2. *J. Biol. Chem.* **284**, 16452–16462 (2009).
- 823 21. Chandrasekhar, K. D., Bas, T. & Kobertz, W. R. KCNE1 subunits require co-assembly with K+
824 channels for efficient trafficking and cell surface expression. *J. Biol. Chem.* **281**, 40015–40023
825 (2006).
- 826 22. Bianchi, L. *et al.* Cellular dysfunction of LQT5-minK mutants: abnormalities of IKs, IKr and trafficking

- 827 in long QT syndrome. *Hum. Mol. Genet.* **8**, 1499–1507 (1999).
- 828 23. Jain, P. C. & Varadarajan, R. A rapid, efficient, and economical inverse polymerase chain reaction-
829 based method for generating a site saturation mutant library. *Anal. Biochem.* **449**, 90–98 (2014).
- 830 24. Rocheleau, J. M., Gage, S. D. & Kobertz, W. R. Secondary structure of a KCNE cytoplasmic domain.
831 *J. Gen. Physiol.* **128**, 721–729 (2006).
- 832 25. Wu, D.-M. *et al.* Characterization of an LQT5-related mutation in KCNE1, Y81C: implications for a
833 role of KCNE1 cytoplasmic domain in IKs channel function. *Heart Rhythm* **3**, 1031–1040 (2006).
- 834 26. Chandrasekhar, K. D. *et al.* O-glycosylation of the cardiac I(Ks) complex. *J. Physiol.* **589**, 3721–3730
835 (2011).
- 836 27. Bas, T. *et al.* Post-translational N-glycosylation of type I transmembrane KCNE1 peptides:
837 implications for membrane protein biogenesis and disease. *J. Biol. Chem.* **286**, 28150–28159
838 (2011).
- 839 28. Kirkton, R. D. & Bursac, N. Engineering biosynthetic excitable tissues from unexcitable cells for
840 electrophysiological and cell therapy studies. *Nat. Commun.* **2**, 300 (2011).
- 841 29. Chen, Y.-H. *et al.* KCNQ1 gain-of-function mutation in familial atrial fibrillation. *Science* **299**, 251–
842 254 (2003).
- 843 30. Peng, G., Barro-Soria, R., Sampson, K. J., Larsson, H. P. & Kass, R. S. Gating mechanisms underlying
844 deactivation slowing by two KCNQ1 atrial fibrillation mutations. *Sci. Rep.* **7**, 45911 (2017).
- 845 31. Restier, L., Cheng, L. & Sanguinetti, M. C. Mechanisms by which atrial fibrillation-associated
846 mutations in the S1 domain of KCNQ1 slow deactivation of IKs channels. *J. Physiol.* **586**, 4179–4191
847 (2008).
- 848 32. Kozek, K. A. *et al.* High-throughput discovery of trafficking-deficient variants in the cardiac
849 potassium channel KV11.1. *Heart Rhythm* **17**, 2180–2189 (2020).
- 850 33. Melman, Y. F., Domènech, A., de la Luna, S. & McDonald, T. V. Structural determinants of KvLQT1

- 851 control by the KCNE family of proteins. *J. Biol. Chem.* **276**, 6439–6444 (2001).
- 852 34. Melman, Y. F., Krumerman, A. & McDonald, T. V. A Single Transmembrane Site in the KCNE-
- 853 encoded Proteins Controls the Specificity of KvLQT1 Channel Gating *. *J. Biol. Chem.* **277**, 25187–
- 854 25194 (2002).
- 855 35. Kuenze, G. *et al.* Allosteric mechanism for KCNE1 modulation of KCNQ1 potassium channel
- 856 activation. *Elife* **9**, (2020).
- 857 36. Li, P. *et al.* Differential modulations of KCNQ1 by auxiliary proteins KCNE1 and KCNE2. *Sci. Rep.* **4**,
- 858 4973 (2014).
- 859 37. Anderson, C. L. *et al.* Large-scale mutational analysis of Kv11.1 reveals molecular insights into type
- 860 2 long QT syndrome. *Nat. Commun.* **5**, 5535 (2014).
- 861 38. Nishio, Y. *et al.* D85N, a KCNE1 polymorphism, is a disease-causing gene variant in long QT
- 862 syndrome. *J. Am. Coll. Cardiol.* **54**, 812–819 (2009).
- 863 39. Kääb, S. *et al.* A large candidate gene survey identifies the KCNE1 D85N polymorphism as a possible
- 864 modulator of drug-induced torsades de pointes. *Circ. Cardiovasc. Genet.* **5**, 91–99 (2012).
- 865 40. Adler, A. *et al.* An International, Multicentered, Evidence-Based Reappraisal of Genes Reported to
- 866 Cause Congenital Long QT Syndrome. *Circulation* **141**, 418–428 (2020).
- 867 41. Glazer, A. M. *et al.* Arrhythmia Variant Associations and Reclassifications in the eMERGE-III
- 868 Sequencing Study. *Circulation* (2021) doi:10.1161/CIRCULATIONAHA.121.055562.
- 869 42. Choi, S. H. *et al.* Rare Coding Variants Associated With Electrocardiographic Intervals Identify
- 870 Monogenic Arrhythmia Susceptibility Genes: A Multi-Ancestry Analysis. *Circ Genom Precis Med* **14**,
- 871 e003300 (2021).
- 872 43. Van Driest, S. L. *et al.* Association of Arrhythmia-Related Genetic Variants With Phenotypes
- 873 Documented in Electronic Medical Records. *JAMA* **315**, 47–57 (2016).
- 874 44. Coyote-Maestas, W., Nedrud, D., He, Y. & Schmidt, D. Determinants of trafficking, conduction, and

- 875 disease within a K⁺ channel revealed through multiparametric deep mutational scanning. *Elife* **11**,
876 (2022).
- 877 45. Weile, J. *et al.* A framework for exhaustively mapping functional missense variants. *Mol. Syst. Biol.*
878 **13**, 957 (2017).
- 879 46. Glazer, A. M. *et al.* Deep Mutational Scan of an SCN5A Voltage Sensor. *Circ Genom Precis Med* **13**,
880 e002786 (2020).
- 881 47. Ng, C.-A. *et al.* A massively parallel assay accurately discriminates between functionally normal and
882 abnormal variants in a hotspot domain of KCNH2. *Am. J. Hum. Genet.* **109**, 1208–1216 (2022).
- 883 48. Hoppe, U. C., Marbán, E. & Johns, D. C. Distinct gene-specific mechanisms of arrhythmia revealed
884 by cardiac gene transfer of two long QT disease genes, HERG and KCNE1. *Proc. Natl. Acad. Sci. U. S.*
885 *A.* **98**, 5335–5340 (2001).
- 886 49. Nakajo, K., Ulbrich, M. H., Kubo, Y. & Isacoff, E. Y. Stoichiometry of the KCNQ1 - KCNE1 ion channel
887 complex. *Proc. Natl. Acad. Sci. U. S. A.* **107**, 18862–18867 (2010).
- 888 50. McDonald, T. V. *et al.* A minK–HERG complex regulates the cardiac potassium current IKr. *Nature*
889 **388**, 289–292 (1997).
- 890 51. Ávalos Prado, P. *et al.* KCNE1 is an auxiliary subunit of two distinct ion channel superfamilies. *Cell*
891 **184**, 534-544.e11 (2021).
- 892 52. Du, C., El Harchi, A., Zhang, H. & Hancox, J. C. Modification by KCNE1 variants of the hERG
893 potassium channel response to premature stimulation and to pharmacological inhibition. *Physiol*
894 *Rep* **1**, e00175 (2013).
- 895 53. Esposito, D. *et al.* MaveDB: an open-source platform to distribute and interpret data from
896 multiplexed assays of variant effect. *Genome Biol.* **20**, 223 (2019).
- 897 54. Karczewski, K. J. *et al.* The mutational constraint spectrum quantified from variation in 141,456
898 humans. *Nature* **581**, 434–443 (2020).

- 899 55. Remillard, C. V. & Yuan, J. X.-J. Activation of K⁺ channels: an essential pathway in programmed cell
900 death. *Am. J. Physiol. Lung Cell. Mol. Physiol.* **286**, L49-67 (2004).
- 901 56. Kowarz, E., Löscher, D. & Marschalek, R. Optimized Sleeping Beauty transposons rapidly generate
902 stable transgenic cell lines. *Biotechnol. J.* **10**, 647–653 (2015).
- 903 57. Mátés, L. *et al.* Molecular evolution of a novel hyperactive Sleeping Beauty transposase enables
904 robust stable gene transfer in vertebrates. *Nat. Genet.* **41**, 753–761 (2009).
- 905 58. Hermann, M. *et al.* Binary recombinase systems for high-resolution conditional mutagenesis.
906 *Nucleic Acids Res.* **42**, 3894–3907 (2014).
- 907 59. Thomas, G. P., Gerlach, U. & Antzelevitch, C. HMR 1556, a potent and selective blocker of slowly
908 activating delayed rectifier potassium current. *J. Cardiovasc. Pharmacol.* **41**, 140–147 (2003).

